SUPPLEMENTARY RESULTS

Figure S1. Mutant p53 Promotes *VEGFR2* Expression in Breast Cancer Cells

(A) MDA-468.shp53 cells were grown in 2D culture condition for 5 days with and without doxycycline (DOX). Total *VEGFR2* transcript was assayed by qRT-PCR and normalized to -DOX condition. Immunoblot at right shows VEGFR2 and mutant p53 protein levels. **(B)** MDA-468.shp53 cells were grown in 3D culture for 8 days with and without doxycycline (DOX). *VEGFR2* transcript from intron 1 was assayed by qRT-PCR and normalized to -DOX condition. **(C)** Immunoblot from MDA-468.shp53 cells grown in 3D culture for 8 days with 0, 5, and 10 μg/mL doxycycline (DOX) to deplete mutant p53. **(D)** SK-BR-3 cells were grown in 2D culture and assayed for *VEGFR2* expression following depletion of mutant p53 with two different siRNAs. Expression is normalized to control siRNA. In each experiment, at least three biological replicates were performed, and the same cell lysates for the extracted RNA were used for immunoblots. Error bars represent standard error. *$p < 0.01$, **$p < 0.001$ by one-tailed t-test.

Figure S2. VEGFR2 Inhibition Phenocopies Loss of Mutant p53

MDA-468.shp53 **(A)**, MDA-231 **(B)**, MCF10A **(C)** and MCF7 **(D)** cells were grown in 3D culture conditions. After 2 days of growth, DMSO vehicle or 5 μM of semaxanib were supplemented to the media. Cells were refed with fresh media and DMSO or semaxanib at day 4. Cells were imaged at day 8. Representative differential interference contrast images were acquired at 10X magnification on live imaging. Scale bar, 100 μm. **(E)** Immunoblot corresponds to cells shown in Figure 2A. MDA-231 cells were transfected with two independent siRNAs to mutant p53 or *VEGFR2* and then grown in 3D culture

conditions for up to 8 days. VEGFR2, mutant p53, and actin loading controls are demonstrated. **(F)** Immunoblot corresponds to cells shown in Figure 2B. MDA-468 cells were transfected with two independent siRNAs to mutant p53 or *VEGFR2* and then grown in 3D culture for up to 8 days. VEGFR2, mutant p53, and actin loading controls are demonstrated.

Figure S3. Mutant p53 Gain of Function is Mediated by *VEGFR2* and Mutant p53 Tumors Respond Better to Cancer Therapy than Wild-Type p53 Tumors

(A) MDA-231 cells were transfected with control siRNA and two independent siRNAs each to deplete mutant p53 or VEGFR2. After trypsinization, approximately 25,000 cells were seeded into culture dishes with Ibidi cell culture-inserts for wound migration, which leaves an approximately 500 μm space where no cells are seeded. 60 hours post-transfection, cells were confluent, and the tissue culture insert was removed. Representative differential interference contrast images were acquired at 10X magnification on live imaging immediately upon removal of the tissue culture insert (0 hours) and at 48 hours. Scale bar, 200 μm. Images correspond to Figure 3D. **(B)** NeoAva clinical trial results stratified by *TP53* status. 79 breast cancer patients with *TP53* wild-type tumors and 38 breast cancer patients with *TP53* mutated tumors were imaged to establish tumor size prior to treatment. Patients were stratified to receive chemotherapy alone or chemotherapy plus bevacizumab. Following treatment, tumor size was analyzed. Each datapoint represents one patient's response to the indicated treatment plotted as the remaining tumor volume divided by the initial tumor volume (which is the response ratio). Data are plotted as a boxplot. The sample size (n) and

median response are indicated. P-value was derived from the Kruskal-Wallis test. **(C)** Table summarizing the total number of tumors that had pathological Complete Response (pCR). Six patients with wild-type p53-containing tumors and one patient with a mutant p53-containing tumor that received chemotherapy did not have tumor measurements before therapy and were excluded from analysis in (**B**) and Figure 3E-F; these patients are included in (**C**) because pCR status is known. **(D)** Average change in tumor volume (response ratio) was plotted by *TP53* status (blue, wild-type *TP53*; red, mutant *TP53*) for patients in the NeoAva study. Response is shown as a continuous variable (ranging from 0-2.34).

Figure S4. Mutant p53 Associates with the *VEGFR2* Promoter and Leads to Promoter Remodeling

(A-C) MDA-468.shp53 cells were cultured for 8 days in 3D culture in the presence (-Mut p53, black) and absence (+Mut p53, red) of doxycycline. Chromatin was crosslinked with formaldehyde and subjected to scanning chromatin immunoprecipiation (ChIP) analysis. Three biological replicates of the ChIP experiment from Figure 4A are shown to demonstrate binding patterns of mutant p53 to the *VEGFR2* promoter along 4 kilobases surrounding the *VEGFR2* transcriptional start site (TSS). ChIP was performed in the presence and absence of doxycycline for mutant p53 and also in the absence of antibodies to p53. Immunoprecipitated chromatin was subjected to qPCR and percent input-normalized signal between -DOX and +DOX samples were plotted relative to the peak binding signal at the -150 bp *VEGFR2* site. **(D)** *In vivo* DNase I footprinting of *VEGFR2* exon 1 in MDA-468.shp53 cells grown in the presence (-Mut p53) or absence

(+Mut p53) of doxycycline to deplete mutant p53. Approximate genomic position is indicated in relation to the transcriptional start site. Densitometry analysis of the relative DNase I hypersensitivity signal is represented by a histogram (+Mut p53, red, -Mut p53, black). Samples were run on the same gel in non-adjacent lanes as indicated by dashed line. **(E)** *In vivo* DNase I footprinting acycloCTP and acycloGTP ladder of the *VEGFR2* genomic region represented in Figure 4C to demonstrate the specificity of the footprinting. Acyclonucleotide ladder primers (Table S4) were used to amplify the genomic region representing the *VEGFR2* promoter region in Figure 4C. Radiolabeled *VEGFR2* promoter footprinting primer 3 was then used along with acycloCTP or acycloGTP-supplemented PCR reaction to perform linear amplification. Footprinting products were resolved on a 6% polyacrylamide/8M urea sequencing gel. The position relative to the *VEGFR2* TSS (+1 site) is indicated. Genome sequence is from the UCSC Genome Browser hg19 assembly.

Figure S5. Mutant p53 Forms a Protein Complex with Members of the SWI/SNF Chromatin Remodeling Complex

(A) Mutant p53 was immunoprecipitated from MDA-468.shp53 cells following chromatin IP procedure. Input represents 3.3% of input material. **(B)** Mutant p53 was immunoprecipitated from MDA-231.shp53 cells following chromatin IP procedure. Input represents 5% of input material. **(C)** Mutant p53 was immunoprecipitated from HT29 cells following chromatin IP procedure. Input represents 25% of input material. Black lines adjoin lanes from the same immunoblot. **(D)** ChIP-re-ChIP workflow. **(E)** Immunodepletion ChIP workflow. **(F)** Immunodepletion ChIP for mutant p53 was

performed in MDA-468.shp53 cells by immunodepleting cross-linked cell extract with p53 or IgG antibodies. ChIP was then performed on the immunodepleted extracts with antibodies to mutant p53 (FL-393 polyclonal p53 antibody) or rabbit IgG control. qPCR was performed at the *VEGFR2* promoter at the site -150 bp from the transcriptional start site. ChIP signal is shown as fold increase over IgG ChIP signal. Error bars represent standard error of two independent experiments.

Figure S6. SWI/SNF is Required for *VEGFR2* Expression and Nucleosomal Remodeling and for the Expression of Select Mutant p53-Dependent Genes

MDA-468.shp53 cells were grown for 5 days in cell culture under the listed experimental conditions. **(A)** Cells grown in the presence (-Mut p53, black) and absence (+Mut p53, red) of doxycycline were fixed with formaldehyde and prepared for scanning chromatin immunoprecipitation. Cell extracts were incubated with anti-p53 antibody FL-393 or a control rabbit IgG. Immunoprecipitated chromatin was subjected to qPCR using primers that spanned the length of the *VEGFR2* gene. Relative position from *VEGFR2* transcriptional start site along with exon position are indicated. Percent input-normalized signal between -DOX and +DOX samples were plotted relative to the peak binding signal at the -150 bp *VEGFR2* site. Error bars represent standard error of three independent experiments. The same samples were used for experiments in Figure 6A-B with immunoblot shown in Figure 6C. **(B-C)** Cells were transfected with 20 nM of two independent siRNAs to deplete **(B)** BRM (red) or **(C)** BRG1 (grey). Expression of three novel mutant p53 transcriptional targets are shown: *IGFBP5*, *ceruloplasmin*, and *mammaglobin-A*. RNA expression was assayed by qRT-PCR and normalized to control

siRNA condition. Error bars represent standard error of three independent experiments. **(D)** Immunoblots for the experiments in (**B**), (**C**), and Figure 6E-I. **(E)** MDA-468.shp53 cells were grown with and without doxycycline to deplete endogenous mutant p53. RNA expression was assayed by qRT-PCR and normalized to control siRNA condition for *IGFBP5*, *ceruloplasmin*, and *mammaglobin-A* genes.

Figure S7. The SWI/SNF Complex is Required for a Sub-Set of Mutant p53 Responsive Genes

(A) Immunoblot for both RNA-sequencing experimental replicates from Figure 7A-B. RNA-sequencing was performed using two independent replicates of MDA-468.shp53 cells grown for 4 days with either control siRNA, siRNA to deplete mutant p53 (Mut p53 knockdown, KD), or siRNAs to co-deplete BRG1 and BRM (SWI/SNF KD). **(B)** Venn diagram of genes regulated by mutant p53 and SWI/SNF. The blue circle represents differentially expressed genes (FDR <0.01) from a published microarray in which shRNA against mutant p53 was induced by doxycycline in MDA-468.shp53 cells grown in 3D cell culture conditions compared to control cells not inducing the shRNA (Freed-Pastor et al. 2012). The red circle represents differentially expressed genes (FDR<0.01) from the same RNA-Seq shown in Figure 7A-B in which MDA-468.shp53 cells (grown in 2D culture) were treated with siRNA against BRM and BRG1 or control siRNA. The results show that 48.83% of the genes regulated by mutant p53 are also regulated by SWI/SNF complexes. **(C)** Hierarchical clustering analysis was performed on the RNA-seq reads from samples described in Figure 7A-B. MDA-468.shp53 cells transfected with control siRNA (siCtrl), siRNA to mutant p53 (sip53), and siRNA to BRG1 and BRM

(siSWI/SNF) in two replicates (appended as 1 or 2) are depicted. This revealed variation in the replicates of siCtrl and sip53 (Mut p53 KD) samples, which did not cluster as shown on the left panel. For correction we used an R package (RUVSeq) which employs the RUVr method that estimates variation by residuals (Risso et al. 2014). After correction the samples clustered as seen on the right panel, and these data were utilized for the RNA-Seq analysis in Figure 7A-B. **(D)** Hierarchical clustering. Samples treated with siRNA against BRG1/BRM (siSWI/SNF; SWI/SNF KD) clustered distinctly from siCtrl.1 and siCtrl.2 before and after correction. For consistency, the clustering depicted on the right panel was utilized for the RNA-Seq analysis.

Table S1. Gene Expression Profiling Identifies VEGFR2 as a Potential Mutant p53 Regulated Gene

Using a 3D tissue culture system, global gene expression profiling was performed in MDA-468.shp53 breast cancer cells that contain a doxycycline-inducible short hairpin RNA (shRNA) to *TP53* (Freed-Pastor et al. 2012). Three independent experiments were averaged, and the top 10 genes that were downregulated upon mutant p53 depletion (and thus are genes mutant p53 may upregulate) at 5% significance are listed with the log2 expression values. *IGFBP5*, *Ceruloplasmin* (*CP*), and *Mammaglobin-A* (*SCGB2A2*) were verified as mutant p53 target genes (see Figure S6E).

Table S2. *TP53* Mutation Categories in the Breast Invasive Carcinoma TCGA Provisional Dataset

TP53 mutation classes were categorized from the Breast Invasive Carcinoma TCGA Provisional dataset. 969 breast tumors that had exome or genome sequencing and RNA-sequencing data were included in the analysis. *TP53* mutations were characterized as wild-type, hotspot missense, non-hotspot missense, or truncation mutations (which includes in-frame deletion, in-frame insertion, frameshift, and nonsense mutations). The frequency of each type of *TP53* mutation is listed.

Table S3. *TP53* Missense Mutation Categories in the Breast Invasive Carcinoma TCGA Provisional Dataset

TP53 mutations was categorized from the Breast Invasive Carcinoma TCGA Provisional dataset. The frequency of missense mutation in *TP53* codons are listed for every occurrence greater than 5 times in the dataset (middle column). Codon 245 is provided separately as it is a hotspot mutant (Feki and Irminger-Finger 2004; Walerych et al. 2012). Not every sample had RNA-sequencing data, so the frequency of missense mutations with RNA-sequencing data is provided in the rightmost column. Missense mutations in codons R175, Y220, G245, R248, and R273 were classified *a priori* for analysis as hotspot mutations, as these are reported to be the most frequently mutated residues in breast cancer (Feki and Irminger-Finger 2004; Walerych et al. 2012). These codons are underlined in the top part of the table and shown separately in the bottom section of the table. The sum total of non-hotspot missense and hotspot missense mutations with RNA-seq data is 126 and 49, respectively (Table S2).

Table S4. Primer, Oligonucleotide, and siRNA List

Real-time quantitative reverse transcription polymerase chain reaction (qRT-PCR) primers, scanning chromatin immunoprecipitation (ChIP) primers, micrococcal nuclease (MNase) PCR and MNase-ChIP primers, *in vivo* DNase I footprinting by ligation-mediated PCR primers and ligation linker sequence, plasmid sequencing primers, RNA sequencing library primers, and siRNA sequences are shown. For the ChIP primers, base pair position is approximate and based on UCSC hg19 genome assembly. For microccocal nuclease primers, total amplicon length was calculated. For the RNA sequencing index primer, the barcode location, which was variable, is indicated.

Table S5. SILAC Mass Spectrometry List of Mutant p53 Interactors

H1299-p53-R282W cells with inducible mutant p53 R282W were grown with and without induction of p53 R282W using stable isotope labeling by amino acids in cell culture (SILAC) and immunoprecipitation was performed as described in Extended Methods. Immunoprecipitated material was processed and analyzed by mass spectrometric analysis as described in Extended Methods. Genes corresponding to mass spectra peptides with H/L normalized ratio > 2.0 are listed along with the official full name and NCBI gene alias. SWI/SNF components are listed in bold. BRM and BRG1 are both listed because an enriched peptide maps to both proteins.

Table S6. BioGRID Analysis of p53 and SWI/SNF Interaction Networks

BioGRID release 3.2.118 (Stark et al. 2006) was utilized to compile lists of *TP53* and SWI/SNF interactors based on published protein-protein or genetic interactions from

human samples. Gene List 1 included *TP53*, for which there were 798 published p53 interactors (not shown). Gene List 2 included the listed SWI/SNF components (SWI/SNF gene aliases are listed) for which there were a total of 417 published SWI/SNF interactors (not shown). From the 798 *TP53* and 417 SWI/SNF interactors, there were 115 genes that overlapped between *TP53* and SWI/SNF groups (Common Interacting Partners). The 115 genes are separated into three columns and listed in alphabetical order. Note that SWI/SNF components and *TP53* are on the list (bolded and underlined), as different SWI/SNF components have been shown to interact with wild-type p53 (see main text). Nine proteins (bolded in red) that have been reported to interact with mutant p53 that are on the list are shown separately with the indicated references, which are listed in the Supplementary References section.

EXTENDED MATERIALS AND METHODS

Breast Tumor Analysis from TCGA Provisional Breast Cancer Dataset

The Cancer Genome Atlas (TCGA) datasets (Network 2012) were downloaded directly from the TCGA data portal (February 2014). The Breast Invasive Carcinoma (BRCA) TCGA Provisional dataset was used for analysis. The datasets were imported into Matlab and data analysis was performed using Matlab scripts (Sobie 2011). First, the somatic mutations dataset was analyzed to determine tumor samples that had mutations in *TP53*. We stratified the tumor samples based on their *TP53* mutational status. The tumor samples that were sequenced for somatic mutations but did not report any mutations in the *TP53* locus are assumed to be wild-type for *TP53*. This dataset included information on the type of mutations in *TP53* such as missense, nonsense, in-frame deletion, in-frame insertion, frameshift and silent mutations. The nonsense, frameshift, in-frame deletion, and in-frame insertion mutations generally produce a truncated, nonfunctional transcript and by this justification were pooled into one group and labeled as truncation mutations. For the purposes of our analysis, missense mutations in residues R175, Y220, G245, R248, and R273 were classified *a priori* as hotspot mutations, as these are the most frequently mutated residues in breast cancer (Table S3)(Feki and Irminger-Finger 2004; Walerych et al. 2012). All other missense mutations were classified as non-hotspot missense mutations. Tumor samples with silent mutations were not considered for the purpose of our analysis. Thus, all tumor samples were stratified on the basis of *TP53* mutational status. Then, the RNA-sequence V2 (RNA-SeqV2) dataset was downloaded and analyzed to determine the

expression levels of genes of interest. In the TCGA portal, the RNA-SeqV2 dataset includes the normalized gene expression of all genes as estimated by upper quartile normalization procedure using the RSEM software package. This data was imported into Matlab and used for analysis. The median gene expression was calculated for each gene of interest following tumor sample stratification based on *TP53* status and plotted using the box plots function. The statistical significance of the findings was determined by Welch's t-test (Jeanmougin et al. 2010). In the case of *VEGFR2* gene, we hypothesized that the gene expression (as determined by RNA sequencing) of tumor samples with hotspot mutations in *TP53* would be higher than other samples. Hence, the one tailed t-test was used in this case. We then extended our analysis to other genes that are also involved in the angiogenic pathway. In this case, we used the two-tailed t-test and corrected for multiple testing by using the false discovery rate procedure (FDR) of Benjamini and Hochberg to obtain the adjusted p-values (Hochberg and Benjamini 1990). The box plots in the figure were plotted in Matlab and are standard box plots with the notch to show the confidence intervals of the median of gene expression. For the sake of visual clarity, the outliers are not displayed on the plot. In the plots, the asterisk (*) symbol denotes statistical significance (p-value < 0.05). The accuracy of the analytical procedure was verified by corroborating multiple samples to the results obtained from the cBioPortal website (Gao et al. 2013).

Micrococcal Nuclease-PCR

Approximately 1.5 million MDA-468.shp53 cells grown in 3D culture conditions were cross-linked for 10 minutes with 1% formaldehyde/PBS at room temperature followed by addition of 2.5 M glycine/PBS to 125 mM final concentration for 5 minutes.

Cells were washed in PBS and harvested by scraping and nuclei were collected via extraction in 10 mL of hypotonic nuclei preparation buffer (300 mM sucrose, 10 mM Tris-HCl, pH 7.5, 15 mM NaCl, 60 mM KCl, 5 mM $MgCl_2$, 0.1 mM EDTA, 0.15 mM spermine, 0.5 mM spermidine, 0.1% Nonidet-P40, 0.5 mM phenylmethyl sulfonyl fluoride) supplemented with 3mM $CaCl_2$ and were pelleted by centrifugation at 500 x g for 5 minutes. Nuclei were resuspended in 350 µL nuclei digestion buffer (300 mM sucrose, 10 mM Tris-HCl, pH 7.5, 15 mM NaCl, 60 mM KCl, 5 mM $MgCl_2$, 0.1 mM EDTA, 0.15 mM spermine, 0.5 mM spermidine, 0.5 mM phenylmethyl sulfonyl fluoride) supplemented with 3mM $CaCl_2$. 0.5 units of micrococcal nuclease (Sigma N3755) diluted in 10 µL of nuclei digestion buffer were added to the sample. Incubation was performed for 10 minutes at 37^{o}C to generate primarily mononucleosomal length DNA fragments as determined by agarose gel electrophoresis. MNase activity was stopped by the addition of EGTA to a final concentration of 20 mM to chelate calcium ions. Chromatin was incubated at 65^{o}C for 5 hours with proteinase K (40 µg proteinase K in 40 µL of Tris-EDTA buffer with 0.5% SDS) to reverse crosslinking and remove protein followed by 1 hour incubation with RNase A (100 units) at 37^{o}C to remove RNA. DNA was extracted with phenol-chloroform-isoamyl alcohol extraction followed by isopropanol precipitation. DNA was resuspended in 40 µL 1X DNA loading dye, and 10 µL of resuspended material was separated via 2% agarose gel electrophoresis. DNA bands were visualized by ethidium bromide staining, and DNA bands corresponding to mononucleosomal-length (~147bp) fragments were excised. DNA was purified with QIAquick Gel Extraction Kit (Qiagen). qRT-PCR was utilized to determine ratio of MNase-resistant DNA between sample conditions. qPCR signal at the *VEGFR2* TSS -

390 to -330 bp site (amplicon 1) was used to normalize -DOX (+Mut p53) and +DOX (-Mut p53) sample qPCR signal. Primers sequences were individually designed and tested for amplification efficiency (Table S4).

In vivo DNase I Footprinting by Ligation-Mediated PCR

Approximately 1.5 million MDA-468.shp53 cells grown in 3D culture conditions were cross-linked for 10 minutes with 1% formaldehyde/PBS at room temperature followed by addition of 2.5 M glycine/PBS to 125 mM final concentration for 5 minutes. Cells were washed in PBS and harvested by scraping and nuclei were collected via extraction in 10 mL of hypotonic nuclei preparation buffer (300 mM sucrose, 10 mM Tris-HCl, pH 7.5, 15 mM NaCl, 60 mM KCl, 5 mM $MgCl_2$, 0.1 mM EDTA, 0.15 mM spermine, 0.5 mM spermidine, 0.1% Nonidet-P40, 0.5 mM phenylmethyl sulfonyl fluoride) and were pelleted by centrifugation at 500 x g for 5 minutes. Nuclei were resuspended in 225 µL nuclei digestion buffer (300 mM sucrose, 10 mM Tris-HCl, pH 7.5, 15 mM NaCl, 60 mM KCl, 5 mM $MgCl_2$, 0.1 mM EDTA acid, 0.15 mM spermine, 0.5 mM spermidine, 0.5 mM phenylmethyl sulfonyl fluoride). 2.5, 5, and 10 units of DNase I (Worthington Biochemical Corporation) diluted in 25 µL of nuclei digestion buffer was prepared separately and supplemented with 5 µL of 100mM $CaCl_2$. 220 µL of the resuspended nuclei were added to DNase I-containing mixtures and gently pipetted. Samples were then moved from ice to room temperature for 4 minutes followed by the addition of 250 µL of lysis buffer (50 mM Tris-HCl, pH 8.0, 20 mM EDTA, 1% SDS, 500 µg/mL proteinase K) to quench the reaction. Chromatin was incubated at 65^{o}C for 5 hours to reverse crosslinking and eliminate protein followed by 1 hour incubation with

RNase A (100 units, Qiagen) at 37^{o}C to remove RNA. DNA was extracted with phenol-chloroform-isoamyl alcohol extraction followed by isopropanol precipitation. DNA was resuspended in Tris-EDTA-buffered water, and DNA concentration was determined by NanoDrop Spectrophotometer (Thermo Scientific).

1 µg of DNA was prepared for single-step primer extension with Footprinting Primer 1 using an annealing temperature of 59 ^{o}C to generate blunt-ended double stranded DNA using VentR (exo-) DNA polymerase (M0257, New England Biolabs) with primers listed in Table S4. Deoxynucleotide triphosphates used in PCR steps were purchased from Roche Applied Science (#11969064001). A linker was ligated to these variable length DNAs using T4 DNA Ligase (Promega M1794) supplemented with ATP (P0759, New England Biolabs) for 12 hours at 16^{o}C to generate DNA fragments of lengths that correspond to the DNase I cleavage site. DNA was purified by ethanol precipitation. A second PCR step using nested Promoter Footprinting Primer 2 (Forward primer) and Footprint Linker Primer (Reverse primer) was utilized to amplify the genomic DNA using PfuTurbo Hotstart DNA Polymerase (#600320, Agilent Technologies) for 30 cycles using a 64.5^{o}C annealing temperature. The Footprint Linker Primer anneals to the variable site in the genomic DNA where DNase I cut and the linker was ligated, allowing the amplification of variably sized products from the genomic DNA. A third nested primer, Footprinting Primer 3, was radiolabeled with [γ^{-32}P]-ATP (PerkinElmer) using T4 polynucleotide kinase (New England Biolabs) and purified from excess [γ^{-32}P]-ATP using microspin G-25 beads (GE Healthcare). PCR was performed at 72^{o}C annealing temperature for 6 cycles with radiolabeled primer 3, which generates linear amplification (because there is no reverse primer) of the *in vivo* footprint sample.

Note that Footprinting Primer 3 is nested within Footprinting Primer 2 and has a higher melting temperature and that Footprinting Primer 2 is nested within Primer 1 and has a higher melting temperature; these considerations offer additional specificity to the genomic amplicon.

Single stranded radiolabeled DNA was resolved by denaturing 8M urea polyacrylamide gel electrophoresis (6% polyacrylamide) and quantitated via phosphorimager exposure. Images were obtained with a Typhoon FLA7000 scanner (GE Healthcare Life Sciences). DNase I hypersensitivity signal represents γ^{-32}P decay detection by phosphorimager-based quantitation that was plotted using densitometry analysis in ImageQuant version 5.2 software (Molecular Dynamics). Primers were individually designed and PAGE-purified (listed in Table S4). Optimal PCR conditions were determined empirically. A GC acyclonucleotide ladder, shown in Figure S4E, was used to confirm that the LM-PCR specifically amplifies the *VEGFR2* proximal promoter region depicted in Figure 4C. Acyclonucleotides were purchased from New England Biolabs (N0460). Procedure was designed with input from other sources (Patterson et al. 1997; Tagoh et al. 2006; Carey et al. 2009).

SILAC Mass Spectrometry

Cell Culture

In stable isotope labeling by amino acids in cell culture (SILAC) experiments, inducible p53 R282W mutant and wild-type p53 expressing H1299 cells were differentially labeled to incorporate isotopic forms of lysine and arginine present in the DMEM media. For triple labeling experiments, the mutant cells were grown in media

containing normal (or 'light' (L)) isotopes of L-lysine-($^{12}C6^{14}N2$) (143 µg/mL, Sigma) and L-arginine- ($^{12}C6^{14}N4$) (83 µg/mL, Sigma) and media containing 'heavy' (H) isotopes of L-lysine-($^{13}C6^{15}N2$) and L-arginine-($^{13}C6^{15}N4$) (Cambridge Isotope Laboratory), respectively. The inducible wild-type p53-expressing cells were grown in media containing an intermediate isotopes (or 'medium' (M)) of L-lysine-(4,4,5,5-^{2}H) and L-arginine-($^{13}C6$) (Cambridge Isotope Laboratory). Cells were grown in SILAC media for at least 5-6 cell doublings to ensure complete incorporation of labeled amino acids. Cells grown in M and H media were then induced with 2.5 µg/mL of Ponasterone A (Invitrogen) for 24 hours before harvesting to induce the expression of p53 R282W and wild-type p53 respectively.

Immunoaffinity Purification of Protein Complexes

Cell pellets were lysed in ice-cold modified RIPA buffer (50mM Tris-HCl, pH 7.5-8, 150mM NaCl, 1% NP-40, Complete, Mini, EDTA-free Protease Inhibitor Cocktail Tablet (Roche) and PhosSTOP Phosphatase Inhibitor Cocktail Tablet (Roche) and centrifuged at 20,000 x g for 20 min at 4ºC. Total protein concentrations were measured using a bicinchoninic acid (BCA) protein assay (Thermo Scientific). For the immunoaffinity experiments, equal quantities of extracts from each differentially labeled cell line were affinity purified separately by overnight incubation at 4ºC with equal amount of anti-p53 (DO-1) conjugated to agarose beads (Santa Cruz Biotechnology). The beads were combined carefully after one wash step in RIPA buffer and were washed for additional three times with RIPA buffer thereafter. To elute the bound proteins from the anti-p53 (DO-1) agarose beads, a 1.5x bead-volume of 2x lithium dodecyl sulfate sample buffer with reducing agent was added and the matrix was boiled

for 5 min. The proteins were separated on NuPAGE 4-12% Bis-Tris gels (Invitrogen) that were then stained with Colloidal Blue (Invitrogen) and destained overnight before being processed for mass spectrometry (see below).

Mass Spectrometry and Data Analysis

Eluted protein complexes were separated by 1D SDS-PAGE and digested with trypsin using published procedures (Shevchenko et al. 2006). Samples were analysed on an Orbitrap or Orbitrap XL (Thermo Fisher) coupled to a Proxeon Easy-nLC. Survey full scan MS spectra (m/z 300 – 1400) were acquired with a resolution of R=60,000 at m/z 400, an AGC target of 1e6 ions, and a maximum injection time of 500 ms. The ten most intense peptide ions in each survey scan with an ion intensity above 2000 counts and a charge state ≥ 2 were sequentially isolated to a target value of 1e4 and fragmented in the linear ion trap by collisionally induced dissociation (CID/CAD) using a normalized collision energy of 35%. A dynamic exclusion was applied using a maximum exclusion list of 500 with one repeat count, repeat and exclusion duration of 30 seconds.

Identification and Quantification of Peptides and Proteins

Proteins were searched using Mascot version 2.2 (Matrix Science, London, UK) against a concatenated target/decoy database prepared by sequence reversing the human International Protein Index (IPI) (version 3.68) with addition of common contaminants such as human keratins, porcine trypsin and proteases. Cysteine carbamidomethylation was searched as a fixed modification, N-acetylation and oxidized

methionine were searched as variable modifications. Labeled arginine and lysine were specified as fixed or variable modifications, depending on the prior knowledge about the parent ion. SILAC peptide and protein quantification was performed automatically with MaxQuant version 1.0.13.13 (Cox and Mann 2008) using default parameter settings. Maximum false discovery rates (FDR) were set to 0.01 for both protein and peptide.

MNase-ChIP

Approximately 10 million sub-confluent MDA-468.shp53 cells were cross-linked for 10 minutes with 1% formaldehyde/PBS at room temperature followed by addition of 2.5 M glycine/PBS to 125 mM final concentration for 5 minutes. Cells were washed in PBS and harvested by cell scraper. Nuclei were collected via extraction in 10 mL of hypotonic nuclei preparation buffer (300 mM sucrose, 10 mM Tris-HCl, pH 7.5, 15 mM NaCl, 60 mM KCl, 5 mM $MgCl_2$, 3mM $CaCl_2$, 0.1 mM ethylenediaminetetraacetic acid, 0.15 mM spermine, 0.5 mM spermidine, 0.1% Nonidet-P40, 0.5 mM phenylmethyl sulfonyl fluoride) and were pelleted by centrifugation at 500 x gravity for 5 minutes. Nuclei were resuspended in 350 µL nuclei digestion buffer (300 mM sucrose, 10 mM Tris-HCl, pH 7.5, 15 mM NaCl, 60 mM KCl, 5 mM $MgCl_2$, 3mM $CaCl_2$, 0.1 mM ethylenediaminetetraacetic acid, 0.15 mM spermine, 0.5 mM spermidine, 0.5 mM phenylmethyl sulfonyl fluoride). 0.5 units of micrococcal nuclease (Sigma N3755) diluted in 10 µL of nuclei digestion buffer were added to the sample. Incubation was performed for 10 minutes at 37^{o}C to generate primarily mononucleosomal length DNA fragments. MNase activity was stopped by the addition of EGTA to a final concentration of 20 mM to chelate calcium ions. Nuclei were disrupted via sonication, cell debris was cleared by

centrifugation, and supernatant was collected. Samples were diluted in RIPA buffer and normalized by DNA content using a NanoDrop Spectrophotometer (Thermo Scientific). Chromatin immunoprecipitation was performed as previously explained using ChIP-grade antibody to Histone H3 (Abcam) or rabbit IgG (Sigma). Following final wash steps, immunoprecipitated chromatin was incubated at 65^{o}C for 5 hours with proteinase K (40 µg proteinase K in 40 µL of Tris-EDTA buffer with 0.5% SDS) to reverse crosslinking and remove protein followed by 1 hour incubation with RNase A (100 units) at 37^{o}C to remove RNA. DNA was extracted with phenol-chloroform-isoamyl alcohol extraction followed by isopropanol precipitation. DNA was resuspended in 30 µL of 1X DNA loading dye. 25 µL of resuspended material was separated via 2% agarose gel electrophoresis. DNA bands were visualized by ethidium bromide staining, and DNA bands corresponding to mononucleosomal-length (~147bp) fragments were excised. DNA was purified with QIAquick Gel Extraction Kit (Qiagen). qPCR was utilized to determine ratio of MNase-resistant DNA between sample conditions. A standard curve of genomic DNA was utilized to determine nanograms (ng) of DNA immunoprecipitated. IP for Histone H3 in the siControl condition at the *VEGFR2* TSS -390 to -330 bp site (amplicon 1) was utilized to normalize samples for the *VEGFR2* TSS -78 to -10 bp site (amplicon 6).

Analysis of RNA-Seq Libraries

FASTQ files containing the reads of individual biological replicates were received from the JP Sulzberg Columbia Genome Center and were processed by trimming barcodes and removing primers using FASTX-Toolkit

(http://hannonlab.cshl.edu/fastx_toolkit). Reads were than mapped by TopHat (Trapnell et al. 2012) to the hg19 reference genome with default settings. Mapped reads were then filtered by quality scores (higher than 10) using SAMTools (Li et al. 2009). To minimize variation between replicates, RUVSeq (R package) was used as described in the manual. Then, edgeR (R package) was utilized to calculate differential gene expression as described in the RUVSeq manual. A Venn diagram program (http://bioinformatics.psb.ugent.be/webtools/Venn/) was used to identify and represent genes that changed between knockdown conditions.

SUPPLEMENTARY REFERENCES

Adorno M, Cordenonsi M, Montagner M, Dupont S, Wong C, Hann B, Solari A, Bobisse S, Rondina MB, Guzzardo V et al. 2009. A Mutant-p53/Smad complex opposes p63 to empower TGFbeta-induced metastasis. *Cell* **137**: 87-98.

Carey MF, Peterson CL, Smale ST. 2009. In vivo DNase I, MNase, and restriction enzyme footprinting via ligation-mediated polymerase chain reaction (LM-PCR). *Cold Spring Harbor protocols* **2009**: pdb prot5277.

Chicas A, Molina P, Bargonetti J. 2000. Mutant p53 forms a complex with Sp1 on HIV-LTR DNA. *Biochemical and biophysical research communications* **279**: 383-390.

Cox J, Mann M. 2008. MaxQuant enables high peptide identification rates, individualized p.p.b.-range mass accuracies and proteome-wide protein quantification. *Nature biotechnology* **26**: 1367-1372.

Di Agostino S, Strano S, Emiliozzi V, Zerbini V, Mottolese M, Sacchi A, Blandino G, Piaggio G. 2006. Gain of function of mutant p53: the mutant p53/NF-Y protein complex reveals an aberrant transcriptional mechanism of cell cycle regulation. *Cancer cell* **10**: 191-202.

Feki A, Irminger-Finger I. 2004. Mutational spectrum of p53 mutations in primary breast and ovarian tumors. *Critical reviews in oncology/hematology* **52**: 103-116.

Frazier MW, He X, Wang J, Gu Z, Cleveland JL, Zambetti GP. 1998. Activation of c-myc gene expression by tumor-derived p53 mutants requires a discrete C-terminal domain. *Molecular and cellular biology* **18**: 3735-3743.

Freed-Pastor WA, Mizuno H, Zhao X, Langerod A, Moon SH, Rodriguez-Barrueco R, Barsotti A, Chicas A, Li W, Polotskaia A et al. 2012. Mutant p53 disrupts mammary tissue architecture via the mevalonate pathway. *Cell* **148**: 244-258.

Gaiddon C, Lokshin M, Ahn J, Zhang T, Prives C. 2001. A subset of tumor-derived mutant forms of p53 down-regulate p63 and p73 through a direct interaction with the p53 core domain. *Molecular and cellular biology* **21**: 1874-1887.

Gao J, Aksoy BA, Dogrusoz U, Dresdner G, Gross B, Sumer SO, Sun Y, Jacobsen A, Sinha R, Larsson E et al. 2013. Integrative analysis of complex cancer genomics and clinical profiles using the cBioPortal. *Sci Signal* **6**: pl1.

Haupt S, Mitchell C, Corneille V, Shortt J, Fox S, Pandolfi PP, Castillo-Martin M, Bonal DM, Cordon-Cardo C, Lozano G et al. 2013. Loss of PML cooperates with mutant p53 to drive more aggressive cancers in a gender-dependent manner. *Cell cycle* **12**: 1722-1731.

Hochberg Y, Benjamini Y. 1990. More powerful procedures for multiple significance testing. *Stat Med* **9**: 811-818.

Jeanmougin M, de Reynies A, Marisa L, Paccard C, Nuel G, Guedj M. 2010. Should we abandon the t-test in the analysis of gene expression microarray data: a comparison of variance modeling strategies. *PLoS One* **5**: e12336.

Lee YI, Lee S, Das GC, Park US, Park SM, Lee YI. 2000. Activation of the insulin-like growth factor II transcription by aflatoxin B1 induced p53 mutant 249 is caused by activation of transcription complexes; implications for a gain-of-function during the formation of hepatocellular carcinoma. *Oncogene* **19**: 3717-3726.

Li H, Handsaker B, Wysoker A, Fennell T, Ruan J, Homer N, Marth G, Abecasis G, Durbin R, Genome Project Data Processing S. 2009. The Sequence Alignment/Map format and SAMtools. *Bioinformatics* **25**: 2078-2079.

Network TCGA. 2012. Comprehensive molecular portraits of human breast tumours. *Nature* **490**: 61-70.

Patterson C, Wu Y, Lee ME, DeVault JD, Runge MS, Haber E. 1997. Nuclear protein interactions with the human KDR/flk-1 promoter in vivo. Regulation of Sp1 binding is associated with cell type-specific expression. *The Journal of biological chemistry* **272**: 8410-8416.

Ragimov N, Krauskopf A, Navot N, Rotter V, Oren M, Aloni Y. 1993. Wild-type but not mutant p53 can repress transcription initiation in vitro by interfering with the binding of basal transcription factors to the TATA motif. *Oncogene* **8**: 1183-1193.

Risso D, Ngai J, Speed TP, Dudoit S. 2014. Normalization of RNA-seq data using factor analysis of control genes or samples. *Nature biotechnology* **32**: 896-902.

Shevchenko A, Tomas H, Havlis J, Olsen JV, Mann M. 2006. In-gel digestion for mass spectrometric characterization of proteins and proteomes. *Nature protocols* **1**: 2856-2860.

Sobie EA. 2011. An introduction to MATLAB. *Sci Signal* **4**: tr7.

Stambolsky P, Tabach Y, Fontemaggi G, Weisz L, Maor-Aloni R, Siegfried Z, Shiff I, Kogan I, Shay M, Kalo E et al. 2010. Modulation of the vitamin D3 response by cancer-associated mutant p53. *Cancer cell* **17**: 273-285.

Stark C, Breitkreutz BJ, Reguly T, Boucher L, Breitkreutz A, Tyers M. 2006. BioGRID: a general repository for interaction datasets. *Nucleic acids research* **34**: D535-539.

Strano S, Fontemaggi G, Costanzo A, Rizzo MG, Monti O, Baccarini A, Del Sal G, Levrero M, Sacchi A, Oren M et al. 2002. Physical interaction with human tumor-derived p53 mutants inhibits p63 activities. *The Journal of biological chemistry* **277**: 18817-18826.

Tagoh H, Cockerill PN, Bonifer C. 2006. In vivo genomic footprinting using LM-PCR methods. *Methods in molecular biology* **325**: 285-314.

Trapnell C, Roberts A, Goff L, Pertea G, Kim D, Kelley DR, Pimentel H, Salzberg SL, Rinn JL, Pachter L. 2012. Differential gene and transcript expression analysis of RNA-seq experiments with TopHat and Cufflinks. *Nature protocols* **7**: 562-578.

Truant R, Xiao H, Ingles CJ, Greenblatt J. 1993. Direct interaction between the transcriptional activation domain of human p53 and the TATA box-binding protein. *The Journal of biological chemistry* **268**: 2284-2287.

Walerych D, Napoli M, Collavin L, Del Sal G. 2012. The rebel angel: mutant p53 as the driving oncogene in breast cancer. *Carcinogenesis* **33**: 2007-2017.

Pfister et al., Supplemental Figure 1

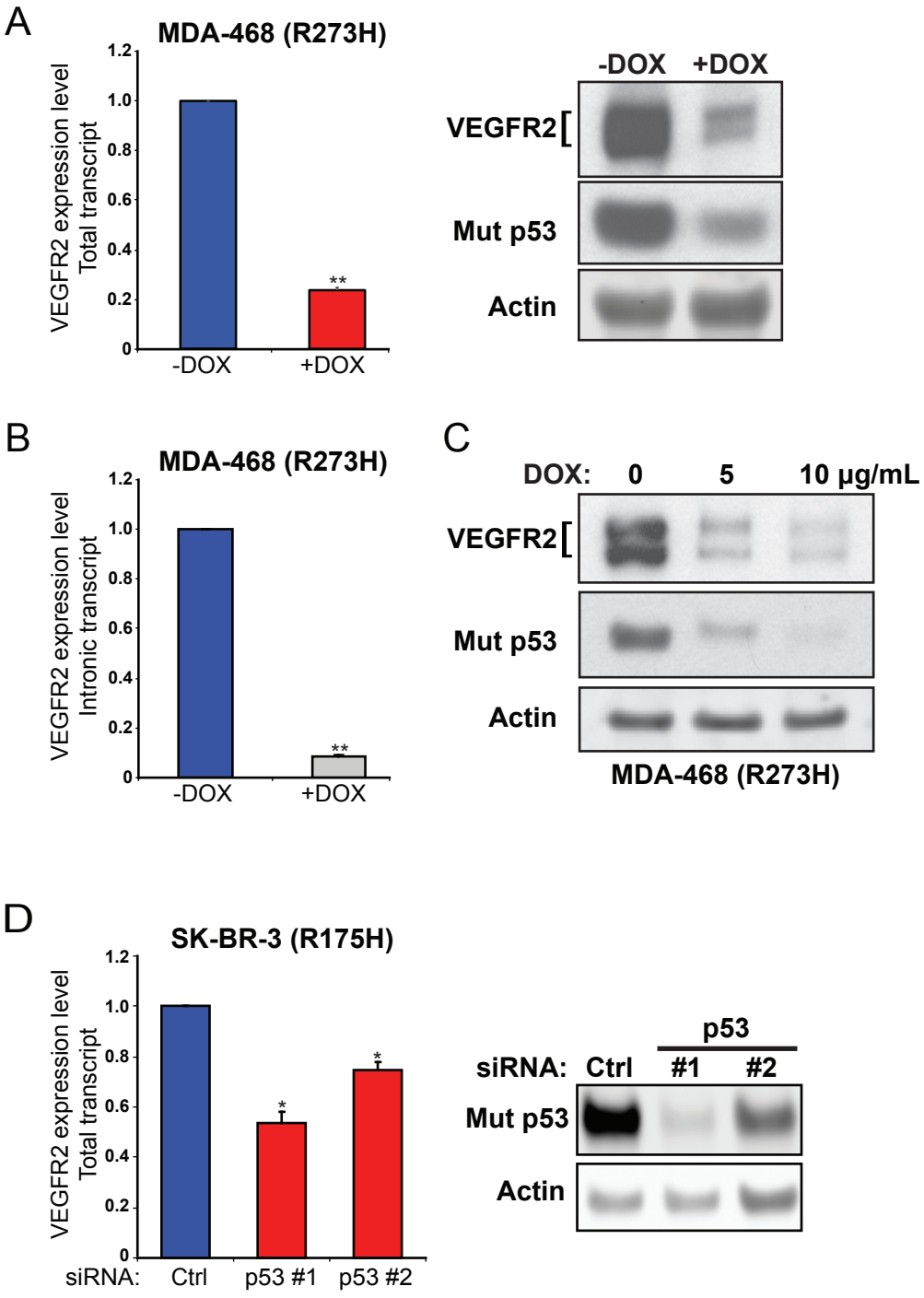

Pfister et al., Supplemental Figure 2

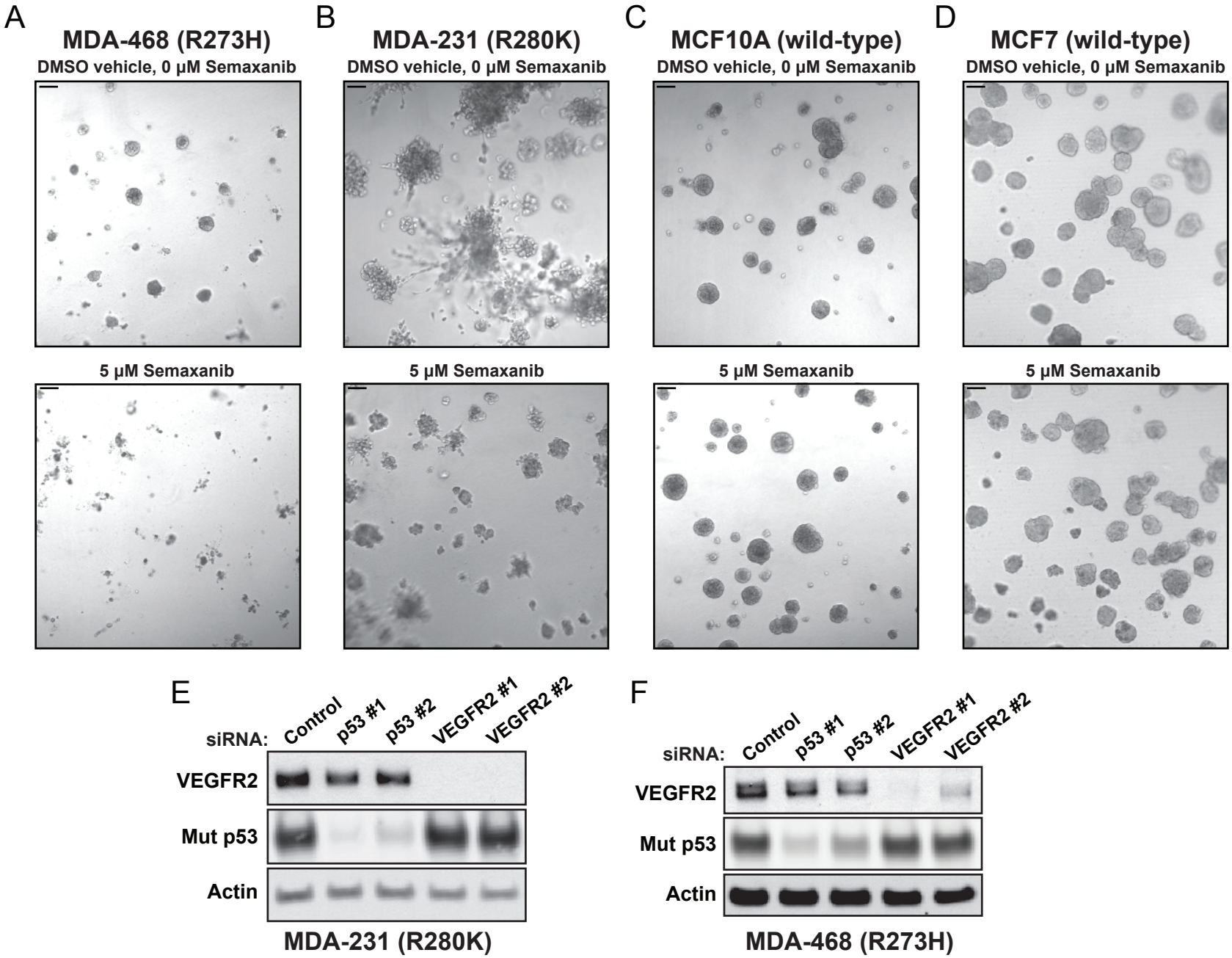

Pfister et al., Supplemental Figure 3

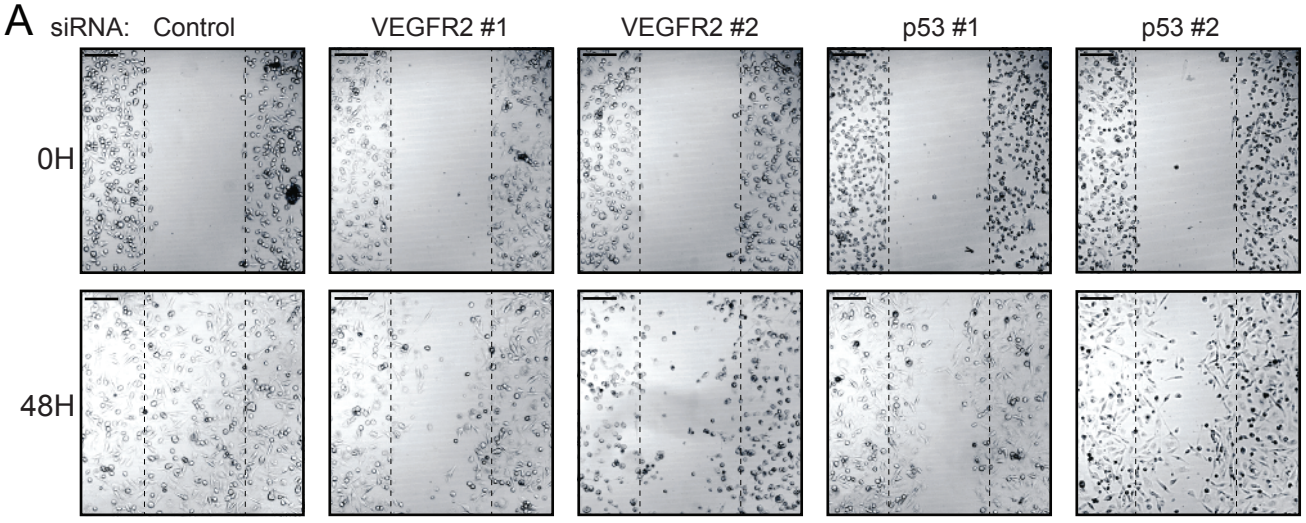

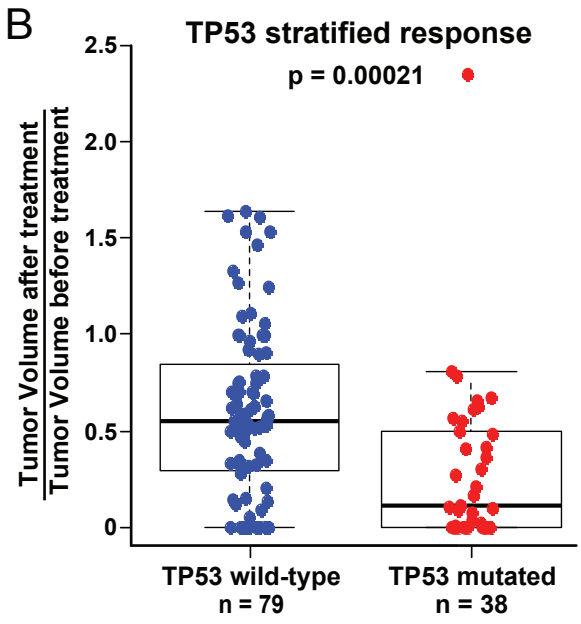

C

Distribution of Complete Responders

Complete responders	TP53 wt (ntot = 85)	TP53 mut (ntot = 39)
Chemo only (n = 62)	2 (of 44) = 4.5%	5 (of 18) = 27.7%
Chemo + Bev (n = 62)	7 (of 41) = 17.1%	7 (of 21) = 33.3%

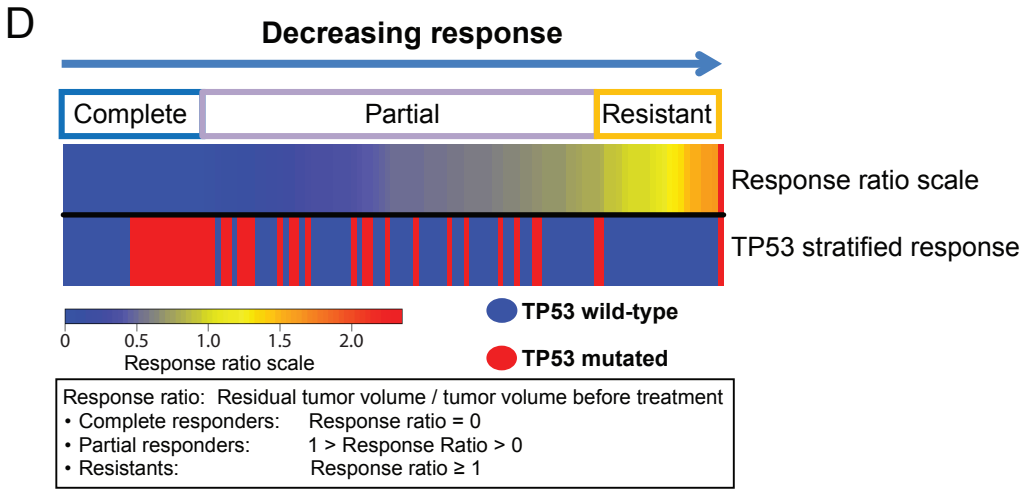

Pfister et al., Supplemental Figure 4

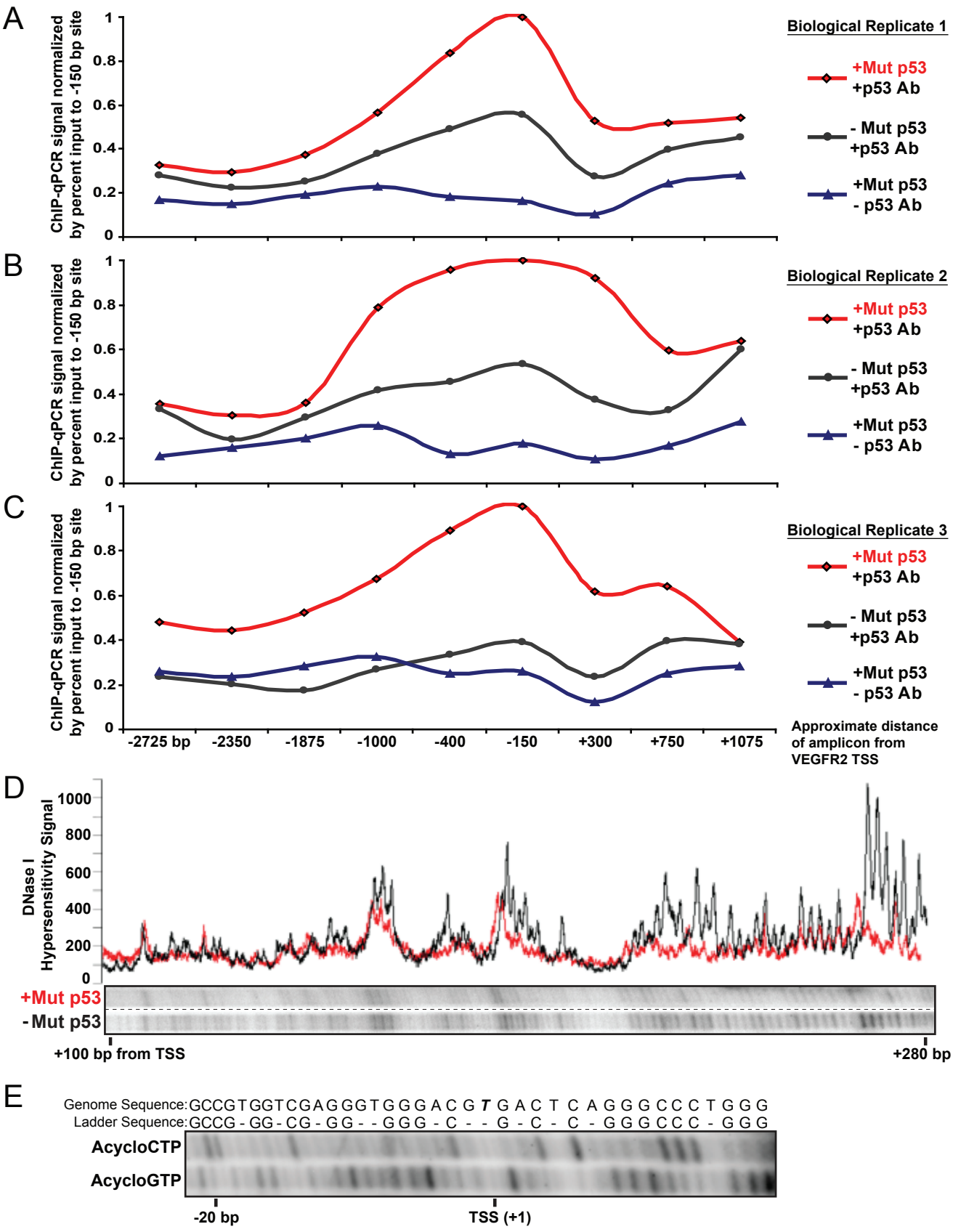

Pfister et al., Supplemental Figure 5

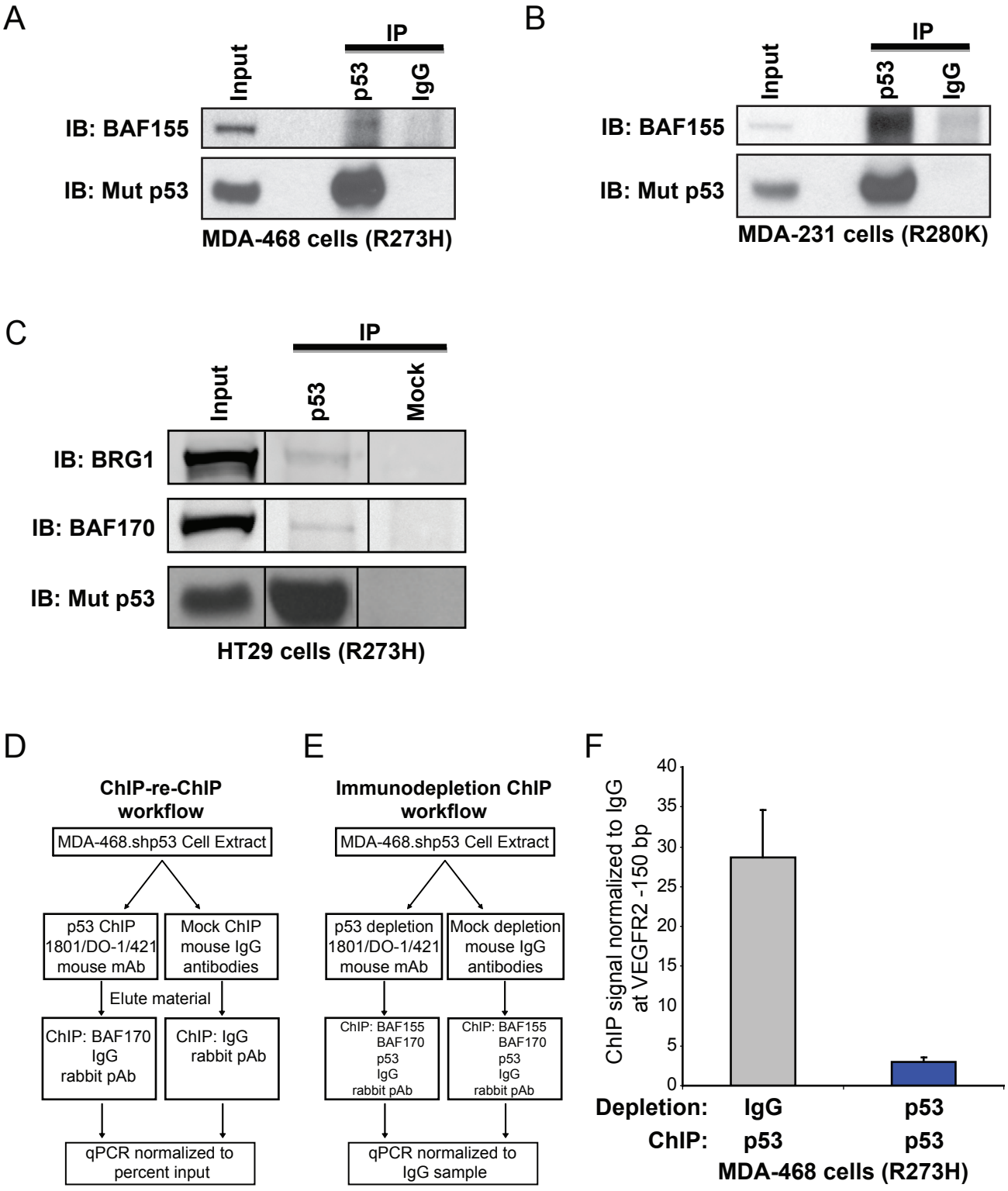

Pfister et al., Supplemental Figure 6

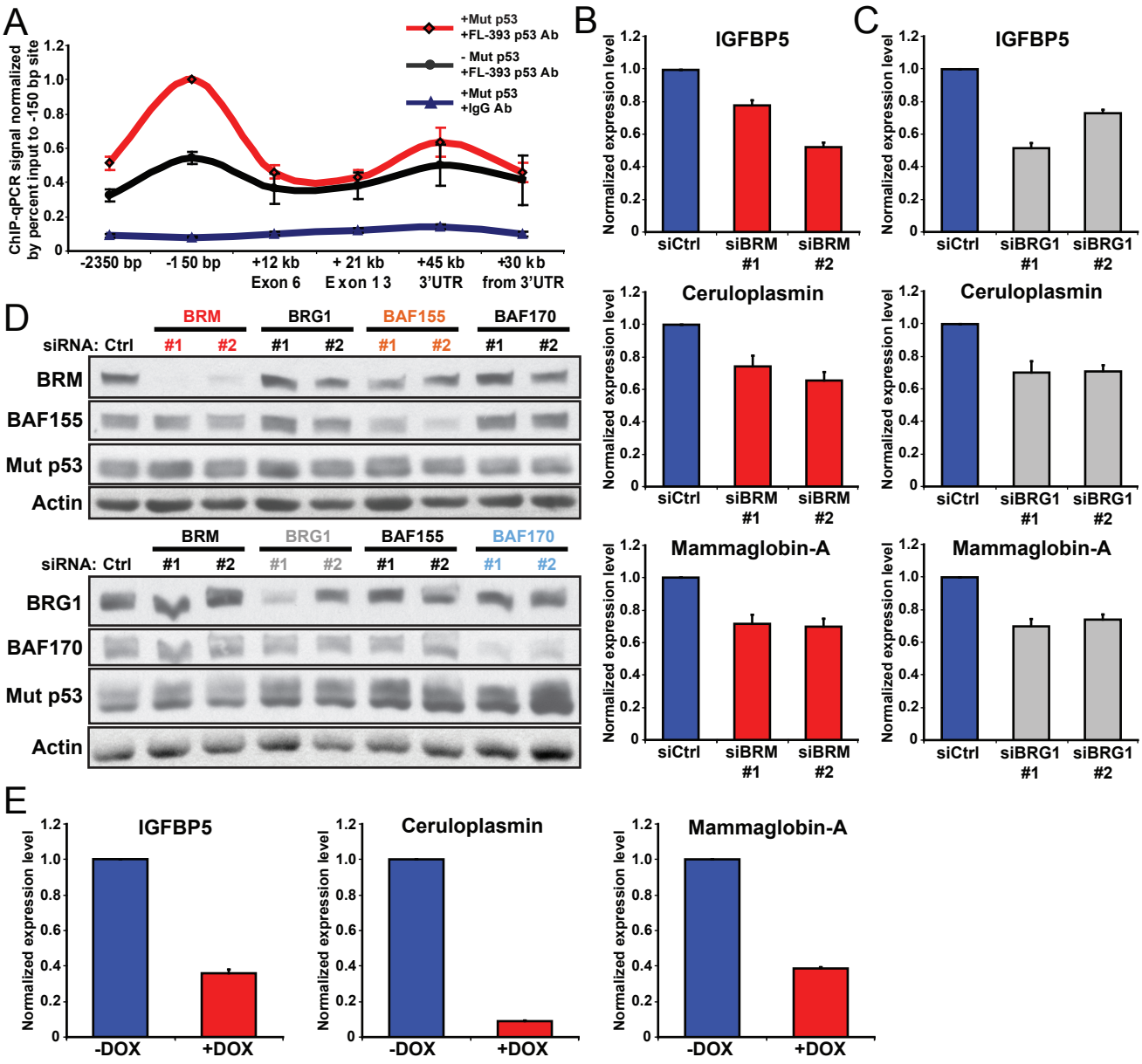

Pfister et al., Supplemental Figure 7

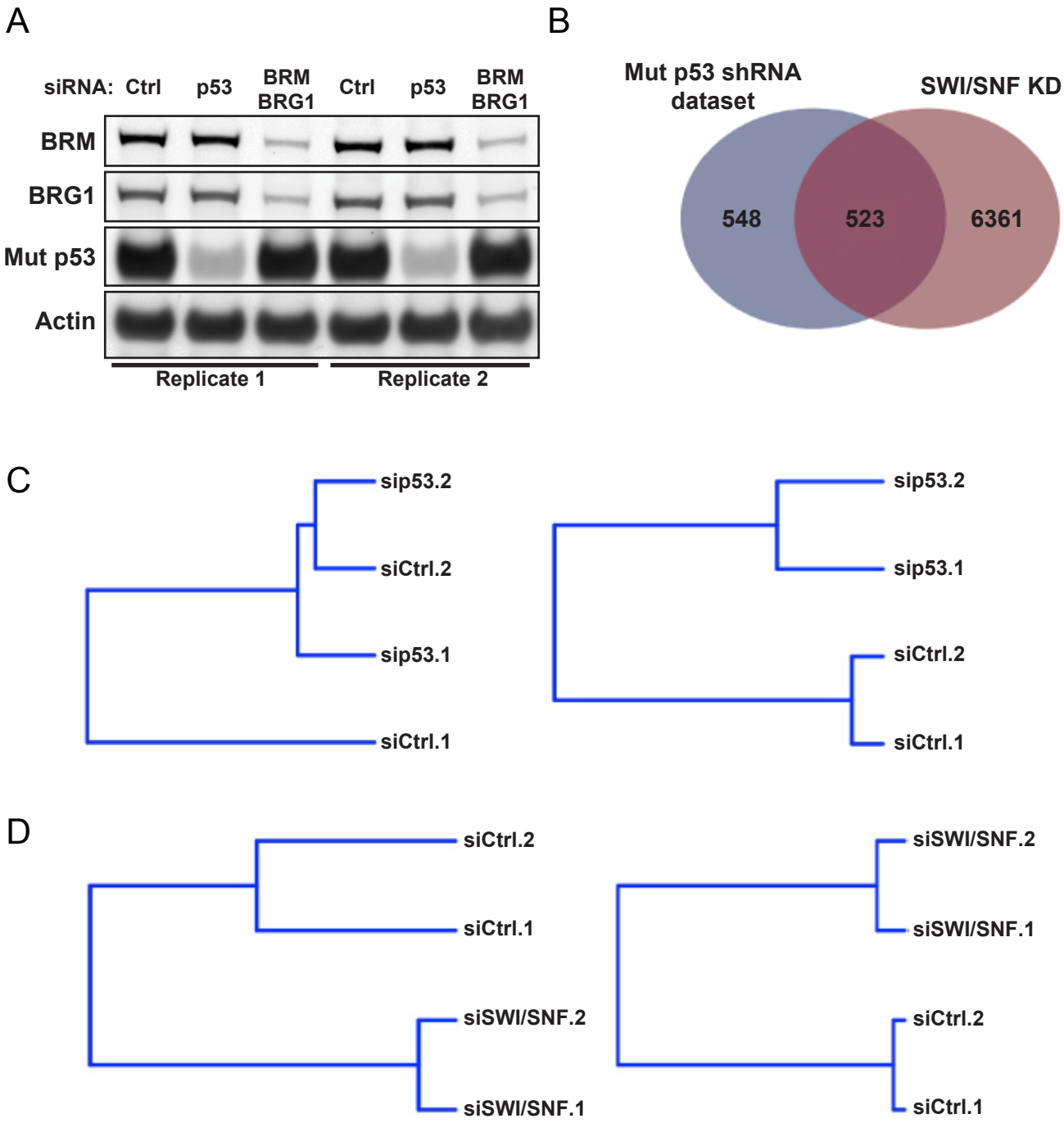

Pfister et al., Supplemental Table 1

Rank	Log2 Change	Gene
1	3.739	IGFBP5
2	2.806	HIST1H2BM
3	2.791	EFEMP1
4	2.765	Ceruloplasmin
5	2.707	Mammaglobin-A
6	2.625	TMPRSS11E
7	2.538	RNU5E
8	2.511	VEGFR2
9	2.414	SAA1
10	2.410	S100A8

Pfister et al., Supplemental Table 2

TP53 Classification	Frequency
Wild-type	672
Hotspot mutation	49
Non-Hotspot missense mutation	126
Truncation mutation	122
Total	969

Pfister et al., Supplemental Table 3

TP53 Missense Mutation	Frequency	Samples with RNA-Seq
175	21	18
273	17	15
193	10	9
248	9	6
220	8	7
176	6	5
132	5	5
179	5	5
194	5	5
195	5	5
286	5	4
245	3	3

TP53 Hotspot Mutant	Frequency	Samples with RNA-Seq
175	21	18
273	17	15
248	9	6
220	8	7
245	3	3

Pfister et al., Supplemental Table 4 (page 1)

	qRT-PCR Primers:	
Forward	*RPL32*	TTCCTGGTCCACAACGTCAAG
Reverse	*RPL32*	TGTGAGCGATCTCGGCAC
Forward	*VEGFR2* exonic primer	CCTCCCCCGCATCACAT
Reverse	*VEGFR2* exonic primer	GCTCGTTGGCGCACTCTT
Forward	*VEGFR2* intronic primer	TCCTTTTCTAGGACTCTGGTTTGC
Reverse	*VEGFR2* intronic primer	CGGCATCTCAGGACATGCT
Forward	*IGFBP5*	GATCTTCCGGCCCAAACA
Reverse	*IGFBP5*	TCTTCACTGCTTCAGCCTTCAG
Forward	*Ceruloplasmin (CP)*	CACCATCAGAGTAACCTTCCATAACA
Reverse	*Ceruloplasmin (CP)*	CCCCAATCGGCTCAATACTG
Forward	*Mammaglobin-A (SCGB2A2)*	TGGCTGCCCCTTATTGGA
Reverse	*Mammaglobin-A (SCGB2A2)*	TTGTATTCAGTCTTAGACACTTGTGGATT

	Scanning ChIP Primers	Sequence:
Forward	*VEGFR2* TSS -2725 bp	CCCAGTTCCTGGTTCAATGC
Reverse	*VEGFR2* TSS -2725 bp	AGCAGGCTCATTCATTCAACAG
Forward	*VEGFR2* TSS -2350 bp	CTACTACTCTGCTGTGGCATCTGAA
Reverse	*VEGFR2* TSS -2350 bp	GCAAAGTGCCCCAAATGTGT
Forward	*VEGFR2* TSS -1875 bp	CTCTCCAAACCAGGTTCCATCT
Reverse	*VEGFR2* TSS -1875 bp	AAATAGGATGGACTCTGGCAAAGT
Forward	*VEGFR2* TSS -1000 bp	TGGTGAAGAATGGTCCTTTAGGTT
Reverse	*VEGFR2* TSS -1000 bp	AATCTTCCAGATGCCTATGTCTTTTAC
Forward	*VEGFR2* TSS -400 bp	TCTCCCTTGTGGCTCCAAAC
Reverse	*VEGFR2* TSS -400 bp	CGCGCGCGTCTGAAG
Forward	*VEGFR2* TSS -150 bp	GTTCTCTCCTGGGCGACTTG
Reverse	*VEGFR2* TSS -150 bp	CCATTTACATCTCCCCATTTCC
Forward	*VEGFR2* TSS +300 bp	TAGACAGGCGCTGGGAGAAA
Reverse	*VEGFR2* TSS +300 bp	AGCAGCACCTTGCTCTGCAT
Forward	*VEGFR2* TSS +750 bp	GCGAGAACAGGCGGTGAA
Reverse	*VEGFR2* TSS +750 bp	GGCCCGGACTAGGATGTTG
Forward	*VEGFR2* TSS +1075 bp	GGTCTCCAAGTAACAGCCAACTG
Reverse	*VEGFR2* TSS +1075 bp	CCACAGCGCTTTGAAAGATG
Forward	*VEGFR2* TSS +12 kb Exon 6	GGAAGTTCAGTCAACTCTTTTTTTCA
Reverse	*VEGFR2* TSS +12 kb Exon 6	TGGGTTTTTAGGTCTCGGTTTACA
Forward	*VEGFR2* TSS +21 kb Exon 13	TTGCAGGACCAAGGAGACTATGT
Reverse	*VEGFR2* TSS +21 kb Exon 13	CGCAATGTCTTTTCTTGGTCTTC
Forward	*VEGFR2* TSS +45 kb 3'UTR	TCTTCTCTCTGCCAACTCCTTTG
Reverse	*VEGFR2* TSS +45 kb 3'UTR	GCTTTTGCTGGGCACCAT
Forward	+30 kb from *VEGFR2* 3'-UTR	GGGCAAAAGGCCTGAACAA
Reverse	+30 kb from *VEGFR2* 3'-UTR	ATTTGCCTTCTTGCCATCTGTATAT

	MNase-PCR and MNase-ChIP Primers		Amplicon
Forward	*VEGFR2* MNase Amplicon 1	TGCAGATTCTCGGCCACTTCAGAC	61 bp
Reverse	*VEGFR2* MNase Amplicon 1	CTCACCAGGCGCGTCAAAG	
Forward	*VEGFR2* MNase Amplicon 2	TCTTCGCAGCGCTCCTGGTGATG	66 bp
Reverse	*VEGFR2* MNase Amplicon 2	GGCGCTGAGCAACTCCAAGATTTAATC	
Forward	*VEGFR2* MNase Amplicon 3	CAGCGCCCGTTACCGAGTAC	64 bp
Reverse	*VEGFR2* MNase Amplicon 3	CAGGAGAGAACATCCCAGAGCAACA	
Forward	*VEGFR2* MNase Amplicon 4	GTTCTCTCCTGGGCGACTTG	68 bp
Reverse	*VEGFR2* MNase Amplicon 4	CCATTTACATCTCCCCATTTCC	
Forward	*VEGFR2* MNase Amplicon 6	CTCCGGCCCCGCCCCGCAT	69 bp
Reverse	*VEGFR2* MNase Amplicon 6	TGGGAGCTGGTGCCGAAACTCTA	
Forward	*VEGFR2* MNase Amplicon 7	GCTCCCACCCTGCACTGAGT	66 bp
Reverse	*VEGFR2* MNase Amplicon 7	AACGCAGCGACCACACATTGA	

Pfister et al., Supplemental Table 4 (page 2)

	***In vivo* DNase I Footprinting by LM-PCR Primers**	
	Blunt end ligation linker sequence #1 (annealed to #1)	AGCTTCGTGAGCATGGTGATCTGAATTC
	Blunt end ligation linker sequence #2 (annealed to #2)	GAATTCAGATC
Reverse	Footprink linker Primer	AGCTTCGTGAGCATGGTGATCTGAATTC
Forward	*VEGFR2* Promoter Footprinting Primer 1	AGGCAGAGGAAACGCAGCGA
Forward	*VEGFR2* Promoter Footprinting Primer 2	AGGAAACGCAGCGACCACACATTG
Forward	*VEGFR2* Promoter Footprinting Primer 3	ACGCAGCGACCACACATTGACCGCTCTC
Forward	*VEGFR2* Exon 1 Footprinting Primer 1	GTCTCCACGCAGAGCCACAG
Forward	*VEGFR2* Exon 1 Footprinting Primer 2	CTCTGCATCCTGCACCTCGAGC
Forward	*VEGFR2* Exon 1 Footprinting Primer 3	TCCTGCACCTCGAGCCGGGCGAAATG
Forward	*VEGFR2* Acyclonucleotide Ladder	ACGCAGCGACCACACATTGACCGCTCTC
Reverse	*VEGFR2* Acyclonucleotide Ladder	GTTGTTGCTCTGGGATGTTCTCTCCTG

	Plasmid Sequencing Primers	
Forward	LNCX Forward Sequencing Primer	AGCTCGTTTAGTGAACCGTCAG
Reverse	LNCX Reverse Sequencing Primer	ACCTACAGGTGGGGTCTTTCATTC
Forward	pcDNA3.1 T7 Forward Sequencing Primer	AATTAATACGACTCACTATAGGG
Forward	VEGFR2 Sequencing Primer-Walk-1	TTCTGTTAGTGACCAACATGG
Forward	VEGFR2 Sequencing Primer-Walk-2	TGAGCACCTTAACTATAGATGG
Forward	VEGFR2 Sequencing Primer-Walk-3	ACTCAAACGCTGACATGTACG
Forward	VEGFR2 Sequencing Primer-Walk-4	CAAGAACTTGGATACTCTTTGG
Forward	VEGFR2 Sequencing Primer-Walk-5	TGATTGCCATGTTCTTCTGG
Forward	VEGFR2 Sequencing Primer-Walk-6	AAGGGAAAGACTACGTTGG
Forward	VEGFR2 Sequencing Primer-Walk-7	TCAGAGTTGGTGGAACATTTG

	RNA Sequencing Library Primers	Barcode location underlined
	5'-Adapter	GUUCAGAGUUCUACAGUCCGACGAUCNNNN
	3'-Adapter	5rApp/NNNNTGGAATTCTCGGGTGCCAAGG/3ddC/
	Reverse Transcription Primer	GCCTTGGCACCCGAGAATTCCA
Forward	Index Forward Primer	AATGATACGGCGACCACCGAGATCTACACGTTCAGAGTTCTACAGTCCGA
Reverse	Index Reverse Primer, contains barcode	CAAGCAGAAGACGGCATACGAGATCGTGATGTGACTGGAGTTCCTTGGCACCCGAGAATTCCA

	siRNA sequences:	Life Technologies Silencer Select ® siRNA Reference	Gene
Sense	GUAAUCUACUGGGACGGAATT	s605	*TP53*
Antisense	UUCCGUCCCAGUAGAUUACCA	s605	*TP53*
Sense	GAAAUUUGCGUGUGGAGUATT	s606	*TP53*
Antisense	UACUCCACACGCAAAUUUCCT	s606	*TP53*
Sense	CAUGUUCUCUAAUAGCACATT	s7822	*VEGFR2*
Antisense	UGUGCUAUUAGAGAACAUGGT	s7822	*VEGFR2*
Sense	CCAUCGUCAUGGAUCCAGATT	s7823	*VEGFR2*
Antisense	UCUGGAUCCAUGACGAUGGAC	s7823	*VEGFR2*
Sense	CCGCAUAGCUCAUAGGAUATT	s13133	*BRM*
Antisense	UAUCCUAUGAGCUAUGCGGGC	s13133	*BRM*
Sense	GCCCAUCGAUGGUAUACAUTT	s13134	*BRM*
Antisense	AUGUAUACCAUCGAUGGGCTT	s13134	*BRM*
Sense	GGAAUACCUCAAUAGCAUUTT	s13139	*BRG1*
Antisense	AAUGCUAUUGAGGUAUUCCTG	s13139	*BRG1*
Sense	GGCUUGAUGGAACCACGAATT	s13140	*BRG1*
Antisense	UUCGUGGUUCCAUCAAGCCTG	s13140	*BRG1*
Sense	CCAACACCUGUACCCAAUATT	s13145	*BAF155*
Antisense	UAUUGGGUACAGGUGUUGGGT	s13145	*BAF155*
Sense	CAAGAGUAUUUAACUAGCATT	s13146	*BAF155*
Antisense	UGCUAGUUAAAUACUCUUGGG	s13146	*BAF155*
Sense	GCUACUAUCCUGACAGUUATT	s13148	*BAF170*
Antisense	UAACUGUCAGGAUAGUAGCCC	s13148	*BAF170*
Sense	GCAAUGCACCGCUCACUAATT	s13149	*BAF170*
Antisense	UUAGUGAGCGGUGCAUUGCTG	s13149	*BAF170*

Pfister et al., Supplemental Table 5

Genes corresponding to Mass Spectra Peptides	Official Full Name	NCBI Gene Alias
ATOH1	Atonal homolog 1	ATH1; HATH1; MATH-1; bHLHa14
ANXA6	Annexin A6	ANX6; CBP68
XPOT	Exportin, tRNA	XPO3
VAPA	Vesicle-associated membrane protein-associated protein A, 33kDa	VAP-A; VAP33; VAP-33; hVAP-33
VAPB	Vesicle-associated membrane protein-associated protein B and C	ALS8; VAP-B; VAMP-B
PEF1	Penta-EF-hand domain containing 1	ABP32; PEF1A
HSPB1	Heat shock 27kDa protein 1	HS.76067; HEL-S-102
NGDN	Neuroguidin, EIF4E binding protein	NGD; LCP5; CANu1; lpd-2; C14orf120
BRM	SWI/SNF related, matrix associated, actin dependent regulator of chromatin, subfamily a, member 2	SMARCA2; SNF2; SWI2; hBRM; NCBRS; Sth1p; BAF190; SNF2L2; SNF2LA; hSNF2a
BRG1 *peptide maps to BRM and BRG1	SWI/SNF related, matrix associated, actin dependent regulator of chromatin, subfamily a, member 4	SMARCA4; SNF2; SWI2; MRD16; RTPS2; BAF190; SNF2L4; SNF2LB; hSNF2b; BAF190A
BAF53A	Actin-like 6A	ACTL6A; Arp4; ACTL6; INO80K; ARPN-BETA
BCL7A	B-cell CLL/lymphoma 7A	BCL7
BCL7B *peptide maps to BCL7A and BCL7B	B-cell CLL/lymphoma 7B	
BCL7C	B-cell CLL/lymphoma 7C	

Pfister et al., Supplemental Table 6

Gene List 1:	Gene List 2:	Gene Alias:
TP53	SMARCA2	BRG1
	SMARCA4	BRM
	ACTL6A	BAF53A
	SMARCC1	BAF155
	SMARCC2	BAF170
	SMARCB1	INI1/hSNF5
	PBRM1	BAF180
	ARID1A	BAF250A
	ARID1B	BAF250B
	ARID2	BAF200
	SMARCE1	BAF57
	SMARCD1	BAF60A
	SMARCD2	BAF60B
	SMARCD3	BAF60C

Common Interacting Partners A-I	Common Interacting Partners I-S	Common Interacting Partners S-Z
ACTB	ITCH	SIRT7
ACTL6A	KAT2A	SMAD1
AR	KAT2B	**SMAD2**
ARID1A	KAT5	**SMAD3**
ATF3	KDM1A	**SMARCA4**
ATM	MAP1LC3B	**SMARCB1**
AURKB	MAPK14	**SMARCC1**
BMI1	MDM2	**SMARCD1**
BRCA1	MED17	**SMARCD2**
CAD	MED21	**SP1**
CARM1	MLL	STK11
CDK2	**MYC**	SUMO1
CDK8	NCOA1	SUMO2
CDK9	NCOR1	TAF1
CDKN2A	NPM1	TAF10
CHD3	NR0B2	TAF6
COPS5	NR3C1	TAF9
CREB1	NR4A1	**TBP**
CREBBP	PCNA	TFAP4
CSNK2A1	PHB	TOP2B
DDX5	**PML**	TOPORS
ECT2	PPP1CA	**TP53**
ELAVL1	PPP1CC	TP53BP1
EP300	PRMT5	**TP63**
EP400	RB1	TRIM28
ESR1	RB1CC1	TRRAP
EWSR1	RBBP4	UBB
H2AFX	RBBP5	UBC
HDAC1	RBBP7	UBD
HDAC2	RBX1	VCP
HDAC9	RFC1	**VDR**
HECW2	RNF2	WDR77
HHV8GK18_gp81	RPA1	WWOX
HIF1A	SART1	XPC
HMGB1	SETD7	YY1
HNRNPA1	SIN3A	ZMIZ2
HSPB1	SIN3B	ZMYND11
ING1	SIRT1	
ING2	SIRT2	

Characterized Mutant p53 Interactor	References reporting mutant p53 interaction partners (see supplemental references):
EP300	(Di Agostino et al., 2006)
MYC	(Frazier et al., 1998)
PML	(Haupt et al., 2013)
SMAD2	(Adorno, et al. 2009)
SMAD3	(Adorno, et al. 2009
SP1	(Chicas et al., 2000)
TBP	(Ragimov et al., 1993; Truant et al., 1993; Lee et al., 2000)
TP63	(Gaiddon et al., 2001; Strano et al., 2002; Adorno et al., 2009)
VDR	(Stambolsky et al., 2010)